GEM TN-92-52

Progress Report on Design and Simulation Studies for a Tungsten and Liquid Argon Forward Calorimeter for the GEM SSC Detector

Michael A. Shupe
John P. Rutherfoord
University of Arizona
Tuscon, AZ 85721

October 25, 1991

GEM is exploring the feasibility of satisfying hermeticity requirements with a relatively compact forward calorimeter quite close to the interaction region. This report explores whether the physics requirements can be met through realistic simulations.

PROGRESS REPORT ON DESIGN AND SIMULATION STUDIES FOR A TUNGSTEN AND LIQUID ARGON FORWARD CALORIMETER FOR THE GEM SSC DETECTOR OCTOBER 25, 1991*

Michael A. Shupe and John P. Rutherfoord
University of Arizona, Tucson, Arizona 85721

ABSTRACT

I. INTRODUCTION

The forward calorimeter sections of a collider detector are used for jet analysis at high $|\eta|$ and for containment of energy near the beam pipe. The latter makes it possible to accurately determine missing transverse momentum. Events with large missing transverse momentum may in further analysis be associated with high energy neutrinos, or the appearance of new physics, such as supersymmetry.

At SuperCollider energies, $|\eta|$ coverage to 5.5 or 6.0 units of pseudorapidity is needed in order to reject physics backgrounds to such processes [1]. η of 5.5 corresponds to an angle of .468 degrees. For the distances being considered for the position of the front face of the calorimeter, 5.00 meters to 15.00 meters from the interaction point, the inner edge of the forward calorimeter is approximately 2.0 centimeters from the beam. In this region, many things are changing rapidly as one approaches the beam: the momenta for interesting particles are growing into the 1 TeV range, the calorimeter cell sizes are shrinking rapidly, jets are Lorentz folding so that their tranvserve size becomes comparable to or smaller than hadronic shower sizes, the instantaneous rate of particles and the specific ionization rate in sensitive detector media are growing rapidly, and the radiation dose at $\mathcal{L} = 10^{33}$ is reaching the range of hundreds of Megarad per standard SSC year in the hottest parts of the calorimeter.

The GEM detector is evolving to favor a forward calorimeter near the limit closer to the interaction region. For this reason we have begun by studying a calorimeter placed with its front face at 5.50 meters from the interaction point. Before attempting to optimize the design on simulated full events, we have been mapping the momentum spectra and angular distributions of single particles (and jets) in the forward region. We have then chosen a baseline design for the forward calorimeter employing tungsten plates and liquid argon gaps, and begun to calculate its response to single particles using GEANT (GHEISHA) simulations with a detailed geometry specification including beam pipe and cryostat structures. The resulting response and resolution function parameterizations can then be used by other GEM simulation groups studying the physics benchmark processes in simplified models of the GEM detector.

II. PARTICLE AND JET SPECTRA

Currently we are running PYTHIA 5.5 to generate collision events, and JETSET 7.3 to fragment jets. Rather than study individual physics processes, we have begun by generating samples of minimum bias events and samples where a hard-scatter minimum P_t threshold of some value (eg. 30.0 GeV/c) has been required. In looking at single particle spectra we have filtered the particles generated so that only those which would show a response in the calorimeter ("observable particles") would be considered. Specifically, partons, decaying particles, and neutrinos, were removed from the sample in single particle plots. Spectra were then accumulated in bands of $|\eta|$ from 0.0 up to 6.0, where the forward calorimeter covers the region from 3.0 to 5.5.

Figure 1 shows the spectra of total momenta for all observable particles, for 5000 minimum bias events corresponding to about $50\mu s$ of SSC running time at $\mathcal{L} = 10^{33} cm^{-2} s^{-1}$. Particles in the forward calorimeter region above $|\eta| = 3.0$ (the half-depth of the plot) populate momenta in sizeable numbers in the range 200 to 500 GeV/c. This will be the ambient spectrum of particles hitting the calorimeter. However, for most physics signals of interest, the detector trigger will have some P_t threshold. Though this and the resulting particle spectra are process dependent, we can get an idea of the kinematically interesting region by simulating

*Work supported by the Texas National Research Laboratory Commission, Proposal Number 072

events with a minimum P_t requirement on the parton-level single hard scattering subprocess. This is easy to implement in PYTHIA, and events with a minimum P_t of 30.0 GeV/c are shown in Figure 2. Once again, 5000 events have been generated, which would result from an SSC running time of about 8 ms. The P_t requirement has created a broader momentum spectrum with a much larger fraction in the total momentum range above 200 GeV/c, roughly indicating the region where the forward calorimeter must be efficient for particles associated with signal events.

Since the forward calorimeter is to be optimized for the measurement of P_t, rather than P, we also plot the P_t spectra of the same particles. These histograms are shown in Figure 1, for minimum bias events, and Figure 2, for a P_t threshold of 30.0 GeV/c. It is clear that the P_t spectra are roughly η independent, and modulated by the dropoff above $|\eta| = 5.0$.

The second mission of the forward calorimeter is to do jet physics at high $|\eta|$. To follow the same optimization scheme as for single particles, we have begun to study the kinematic properties of jets in this region. (There has been no time to do production running of simulated jets into the simulated forward calorimeter as of yet.) To explore the same questions for jets, we have taken the samples of PYTHIA events described above and plotted the P spectra of minimum bias events in Figure 2 and for 30.0 GeV/c P_t threshold in Figure 1. The corresponding P_t plots are in the same figures. The plots with the P_t threshold requirement show that jets of interest will be populating the P range above 500.0 GeV/c and the P_t range above 30.0 GeV/c (reflecting the generated trigger bias).

The simulation work described below is a program to map out the response function of candidate forward calorimeter designs in these ranges of particle and jet P and P_t.

III. BASELINE CALORIMETER DESIGN

For missing P_t physics, the desirable properties of a forward calorimeter are good P_t resolution and coverage to high $|\eta|$. These same properties tend to lead to good jet resolution, but at present we are not sure whether missing P_t or jet physics requirements will be driving the design, although we expect this to become clear as simulation progresses. To get started, we have developed a baseline design from the following constraints, and will "discover" its properties in simulation:

1) The most recent design study for costing purposes is shown in Figure 3. It is slightly further from the interaction point, at 6.9 m, than the one studied in the current paper (5.5 m). Getting all these parameters to correspond exactly will be part of the design iteration process. The forward calorimeter periodic structure consists of fairly thick (13mm) tungsten plates transverse to the beam, with a thin (1mm) LAr gap between each plate and the next. Each gap is read out by a thin (.2 mm) electrode structure of copper pads on Kapton film to form projective cells and extract the signal to the outer edge of the calorimeter, where the preamps will reside, immersed in the liquid argon. Each unit cell (plate, gap, and pad thickness) is 3.77 radiation lengths, X_o, and 0.139 nuclear absorption lengths, λ, of material. We have begun by simulating a relatively shallow detector, with 72 unit cells, of total depth 10 λ, but will be investigating depths of up to 14 to 16 λ to probe the dependence of detector performance on depth. The rationale for the thin LAr gaps is to minimize the time required to sweep all ionization from the gaps (positives in particular), and to keep the longitudinal dimension of the calorimeter small. This thin gap leads to a small sampling fraction, which in turn worsens the stochastic term contribution to the resolution, but at the high momenta of interest, we expect this term to be negligible (one of the issues we focus on in simulation).

2) The transverse segmentation of the calorimeter follows different criteria from those used in the barrel and endcap calorimeters. To begin with, the choice of tungsten was made not only to keep the forward calorimeter shallow; but, more importantly, to minimize the transverse spread of hadronic showers. Tungsten, though expensive (approximately \$25/lb) is a practical choice for the forward calorimeter because the tonnages are relatively small: 40.0 to 60.0 tons per end for a near calorimeter, depending on depth.

Once the absorber is chosen, the transverse position resolution is determined by the pad structure. In the GEM central and endcap calorimeters, the segmentation will probably be into projective towers with EM tower sizes of $\Delta\eta \times \Delta\phi = .04 \times .04$, and hadronic towers of $\Delta\eta \times \Delta\phi = .08 \times .08$. This hadronic segmentation is driven by particle isolation requirements and by jet resolution. Jets typically are calculated assuming they are contained in a cone with a half angle of 0.7 in $\Delta\rho = \sqrt{(\Delta\eta^2 + \Delta\phi^2)}$, whereas their "cores" are usually within $\Delta\rho = 0.2$ of the parton direction. To see how these segmentations map into three dimensional space in the region of the forward calorimeter, one need only consider the partial derivative $d\eta/d\theta = 1/sin\theta \approx 1/\theta$. If the face of the calorimeter is at fixed z, then the bins of constant $\Delta\theta$ are becoming very small. Or roughly

speaking, we are entering the region where jet sizes are comparable to or smaller than the showers from the hadrons associated with them. (Future reports will contain full description of studies we are making of jet shapes.)

For this reason, we have let the pad sizes be determined largely by hadronic shower size once this "crossover" point is reached. Since our jet studies are not complete, and this remains to be completely quantified, the pad sizes are at the moment a "best guess" based on the shower profiles which have been calculated, combined with back-of-the-envelope calculation. Figure 4 shows the pad patterns which have been chosen for the three depths of the baseline design. The upper pattern is used for the first depth, and the lower for the other two.

3) Depth segmentation of the forward calorimeter is based on several criteria. The first depth is shallow: approximately .84 λ, or 23 X_o. Its purpose is to contain the energy of gammas (and electrons). The plate and gap construction of this section does not differ from the others, hence it has the same sampling fraction and e/h response ratio. It has NOT been optimized for electromagnetic shower resolution. The aim is to be able to get an indication of the fraction of prompt electromagnetic energy in the jet resulting from jet π^o's decaying to photons, and use this fraction to apply a weighting factor correction for the e/h response of the calorimeter. This will not help the fluctuations due to π^o's appearing in showers deeper in the calorimeter (i.e. individual particle EM fraction fluctuations), but it will reduce the effect on the resolution of jets fluctuating in their number of π^o's (jet EM fraction fluctuations). This effect, and the quality of the correction, will be studied as simulation progresses.

The second depth extends to 3.0 to 5.0 λ from the front of the calorimeter. This depth is being tuned to a different criterion. If the momentum resolution of the forward calorimeter is maintained within expected bounds, the P_t resolution will be dominated not by the dP/P term, but by $d\theta/\theta$. The θ resolution is affected, among other things, by transverse fluctuations in hadronic shower development. With reduced absorption length, tungsten is an improvement over lead in this regard, since the overall shower size is smaller. However, the transverse fluctuations deep in the shower are sufficiently large that one gets a worse determination of the shower centroid by including all of the shower than by truncating the sum closer to the front of the calorimeter. The depth of the second section will be optimized using the criterion of optimized centroid resolution.

The third depth is meant to contain shower tails, including those from late developing showers. Longitudinal shower leakage degrades the momentum resolution, and contributes both to the stochastic and constant terms. The total depth of the calorimeter will be optimized so that the fluctuations due to longitudinal shower leakage are well below those due to other sources.

There is a possible need for a fourth section of to be instrumented as a tail-catcher. Its purpose would be not so much to improve the calorimeter resolution as to provide a measure of what is leaking into the most forward areas of the muon detector. It might be used, for example, as a veto. This raises the possibility also, that if the final optimized calorimeter is too shallow to absorb punchthrough to the muon system, additional dead material could be placed behind it.

IV. GEANT 3.14 SIMULATIONS

The program CALSIM is a framework which emphasizes simple specification of plate calorimeters with repetitive plate and gap structures, and calls GEANT routines to simulate electromagnetic and hadronic showers. The geometry is specified in a few lines of the CALSIM input file. A "unit cell" is described by specifying the thicknesses, materials, and order; of absorber, gaps, and electrodes. If desired, cladding material for the absorber, and pad material for the electrodes, may be specified. The whole calorimeter is then built up out of repetitions of this unit cell structure. At present only one such structure may be studied, but extensions in the future will allow for several calorimeter depth sections to be set up in the same simulation (eg. EM, HCAL1, HCAL2, TAIL,...). In the current version of CALSIM, massless gaps and cryostat walls may also be specified in the input deck. The work described in this paper has used the "forward calorimeter" form of CALSIM geometry, where an outer radius, beam pipe hole, and beam area cryostat structures are introduced.

The current work has been done with GEANT 3.14. The list of switch settings is as follows: PAIR 1, COMP 1, DRAY 1, ANNI 1, BREM 1, HADR 3, PHOT 1, MULS 2, LOSS 3, DCAY 1, MUNU 0, and PFIS 1. In addition, the cutoffs have been lowered considerably from the defaults provided as GEANT defaults: CUTGAM = .00001, CUTELE = .00001, CUTNEU = .0001, CUTHAD = .0001, CUTMUO = .001, BCUTM = .0001, BCUTE = .00001, and DCUTE = .00001. Step sizes have also been reduced: DMAXMS = .02, DEEMAX = .05, EPSIL = .001, STMIN = .001. The

electromagnetic settings and cuts are the same as those used by the GEM collaborators simulating accordion electromagnetic calorimeters. They lead to long running times, and have not been studied methodically up to the present. These routines have been run at the University of Arizona on both VAX 3100 series computers and SGI 4D/35's. A few runs have been made on both machines to check for numerical differences, but most of the production has been on the Silicon Graphics machines. To cover as many points as possible, most have been run with 500 simulated events, but some with 1000. The errors quoted on stochastic term resolutions are the consequence of these limited statistics.

The absorber plates, liquid argon gaps, and other structures are defined as standard GEANT volumes. However, the pad structures are defined in a separate user initialization routine. Similarly, the energy deposited in each pad for each event is summed in the user routine GUSTEP, which is called each time a shower particle steps within the detector space. The x, y, and z positions of a shower particle are known at each step, as is the energy deposit associated with that step (DESTEP). These positions are used to find the eta, phi, and depth indices of the pad where the ionization will be collected. The sums are done two ways: for the liquid argon gaps alone (the as in the experiment) and including the absorber plates. In this way the effects of sampling fraction and frequency on the resolution may be separated from the effects of transverse segmentation, by treating the absorber as if it were live material.

V. GEANT AND THREE DIMENSIONAL DISPLAYS

To help insure that the simulations are working properly, and to visualize the shower development in the realistic geometry, we used two types of displays. The first type is generated by GEANT display utility routines, and shows the defined GEANT volumes and the individual charged and neutral particles in the shower superimposed on a phi slice of this geometry. Figure 5 shows a 50 GeV/c pion shower in the detector in one such event.

The second display was written from scratch in the DI3000 display language, and shows the pulse heights in calorimeter cells in a 3D view of the detector where energy deposition is represented by "legos" blocks built on the pad structure of each detector depth. Since the pads are ganged projectively, the pad positions in the center of each ganged depth are used in the display. A typical 200 GeV/c pion shower near the beam pipe is shown in Figure 6. The upper portion of the figure shows the energy deposited in the liquid argon gaps, and the lower portion, in the gaps and absorbers binned into the same pad structure. It is apparent from this display that there are a large number of very soft (negligible) photons which spread transversely through the detector and tend to interact in the absorber material rather than the gaps. For the analysis done in the present paper, the momenta and P_t of showers were calculated by sums over the cells–such as those shown in this display. It is this transverse and depth granularity which contributes to the observed resolutions in P and P_t.

VI. SINGLE PARTICLE RESPONSE FUNCTIONS

To the present, the simulations of the tungsten/LAr forward calorimeter have focussed on the response of the baseline design to single pions. This is because it is most urgent for other GEM simulation studies to know the hadronic single particle response function. The first quantities studied were the linearity and resolution at a point in the calorimeter away from the beam line but also well within the outer rim. Simulated charged pions at 2, 50, and 200 GeV/c were directed at $\eta = 3.6$ into the forward calorimeter. As noted above, shower

The linearity is shown in Figure 7. Note that the brackets shown are not errors on the determination of the mean, but instead indicate the RMS width of the momentum observed in the detector. The calibration constant used to convert energy observed in the gaps to total energy was .003825, the calibration constant for 200 GeV/c. The observed nonlinearity is very small, and will be quantified once the simulations have been run for sufficient statistics.

The energy resolution σ/E at these same points is shown in Figure 8. There appears to be a larger constant term than expected in the resolution associated with these points: perhaps as much as 4% to 5%. Again, fits will be done and reported as more statistics have been accumulated and as we have time to run full studies on deeper versions of this calorimeter (up to 14 λ).

The next step in simulation was to take a first look at the behavior of the response function and resolution as the particle is swept toward the beam pipe. For this purpose, 200 GeV/c pions were directed at η's of 3.69, 4.95, 5.25, and 5.55. Since the inner edge of the pads closest to the beam is at $\eta = 5.5$, we wanted to see how fast these functions would show the effects of the beam region being nearby. Figure 9 shows the single particle

response beginning to "detect" the beam by $\eta \approx 5.0$, and down to half its original value by $\eta = 5.5$. Once again, the brackets in this Figure indicate RMS widths of the momentum distribution, and show the resolution degrading in this same region near the beam.

For most processes of interest, the quantity one would really like to know is the fractional transverse momentum resolution: $d(P_t)/P_t$. This is shown in Figure 10. This function stays near 10% out to an η of 5.0, then worsens rapidly to about 25% at the highest η point calculated.

VII. DIRECTIONS FOR FUTURE WORK

There are definite paths to pursue in this investigation. We will coordinate the simulations closely with the integration work as it progresses to keep the forward calorimeter dimensions, placement, and materials realistic. We will vary the transverse (pad) and longitudinal (depth) segmentations to get the required optimization between cost and the resolution required to measure missing P_t and forward jets. Jets and jet spectra will be generated using both PYTHIA and ISAJET for comparison, and the jet response function mapped out in the same sense as the single hadron spectrum is being mapped now. Electronic noise and event pileup will be added. Analysis at this point will require the introduction of a realistic cluster and jet finder. All along, the simulation will be updated to reflect the latest electrode and pad designs being developed in simultaneous design work. And as the endcap calorimeter becomes better defined, the transition region will be simulated and mapped. Progress has been made in understanding the response of a realistic baseline design, but much remains to be done as the GEM forward calorimeter design evolves.

[1] F.E. Paige and E.M. Wang, *Tuscaloosa Calorimetry Workshop*, (1990).

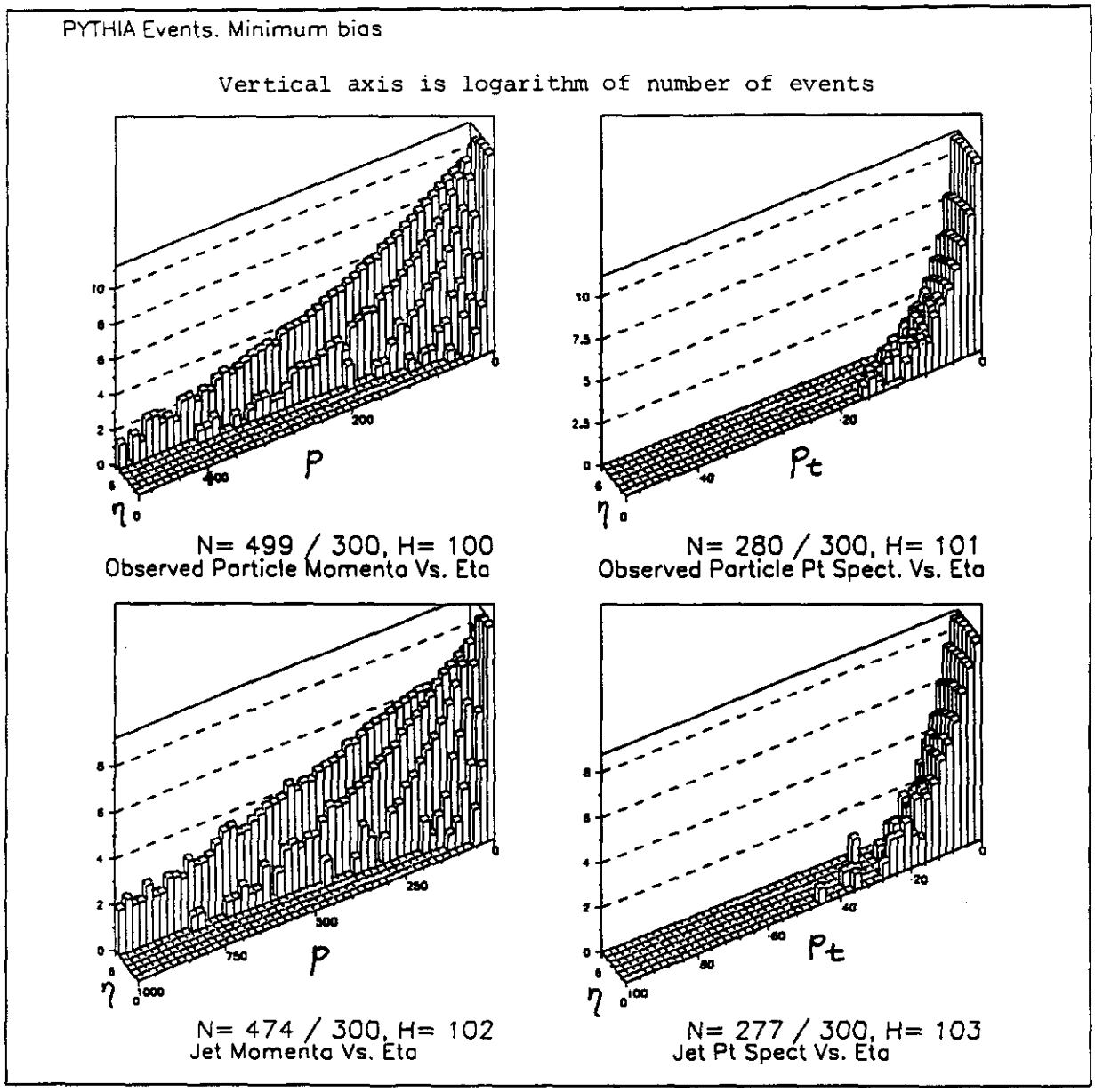
PYTHIA Events. Minimum bias
Vertical axis is logarithm of number of events
P
η
N= 499 / 300, H= 100
Observed Particle Momenta Vs. Eta
Pt
η
N= 280 / 300, H= 101
Observed Particle Pt Spect. Vs. Eta
P
η
N= 474 / 300, H= 102
Jet Momenta Vs. Eta
Pt
η
N= 277 / 300, H= 103
Jet Pt Spect Vs. Eta

Figure 1

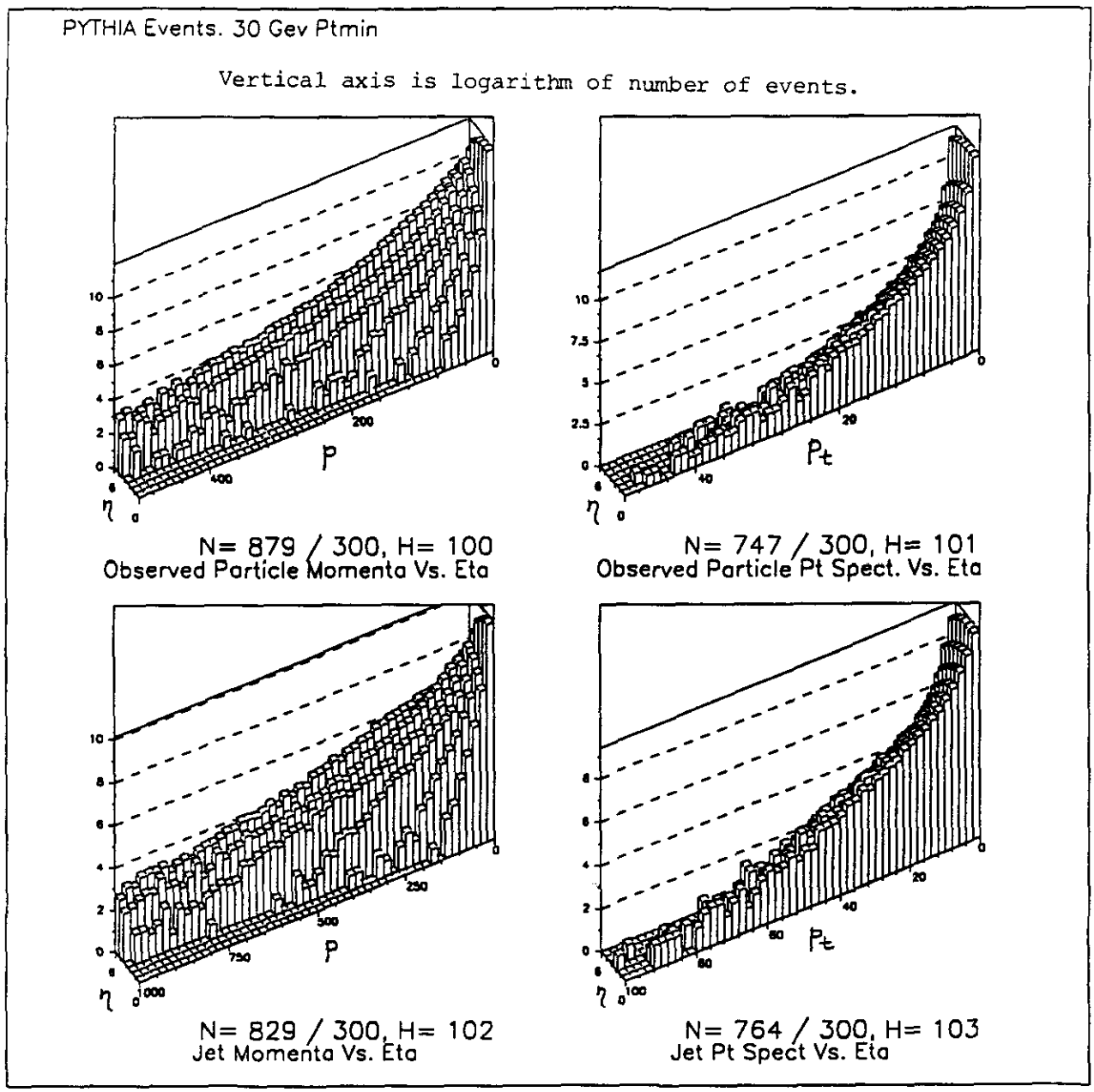
PYTHIA Events. 30 Gev Ptmin
Vertical axis is logarithm of number of events.
P
η
N= 879 / 300, H= 100
Observed Particle Momenta Vs. Eta
Pt
η
N= 747 / 300, H= 101
Observed Particle Pt Spect. Vs. Eta
P
η
N= 829 / 300, H= 102
Jet Momenta Vs. Eta
Pt
η
N= 764 / 300, H= 103
Jet Pt Spect Vs. Eta

Figure 2

Figure 3

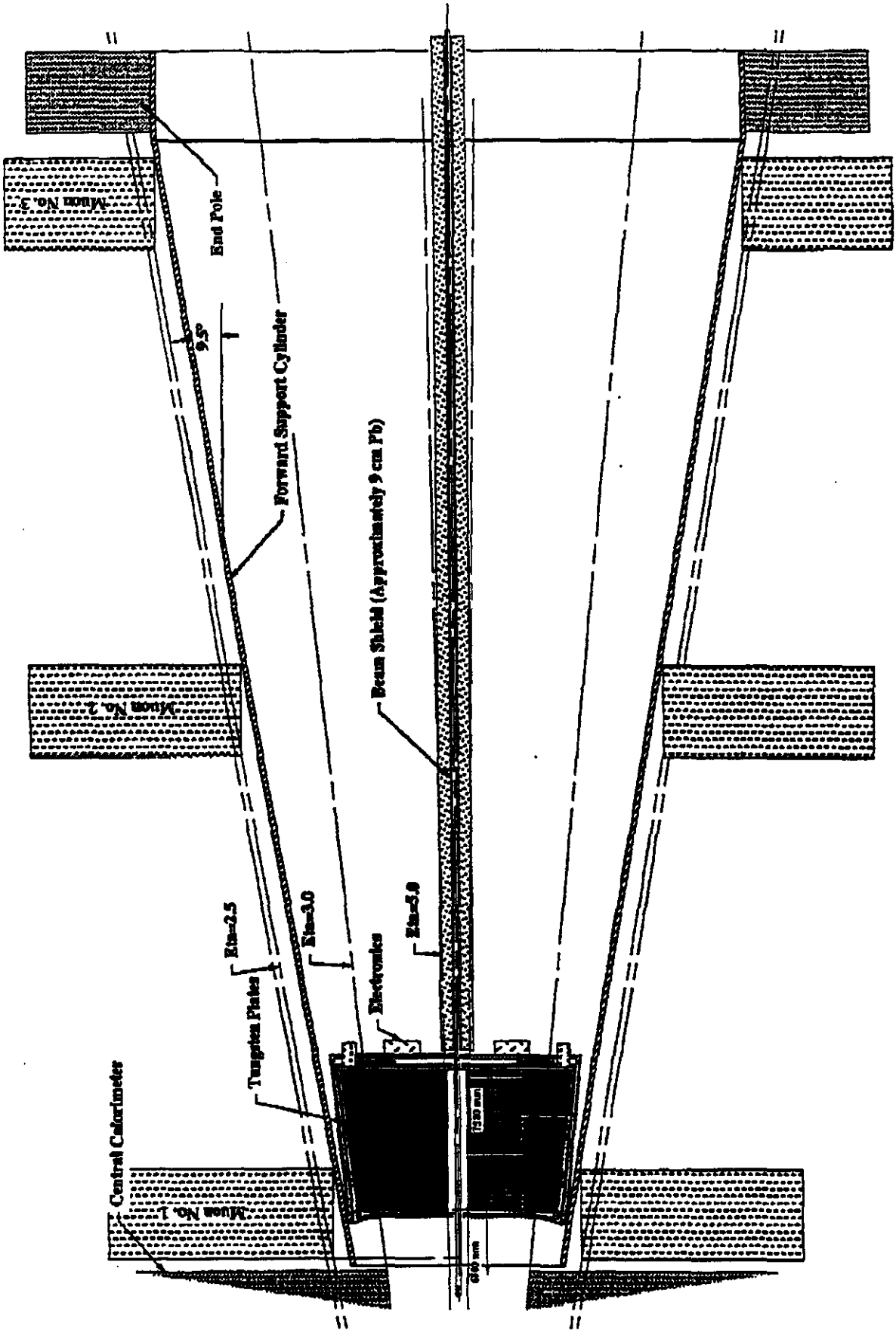

GEM
Forward Calorimeter
Liquid Argon

Rennich

G.03.FD.00015

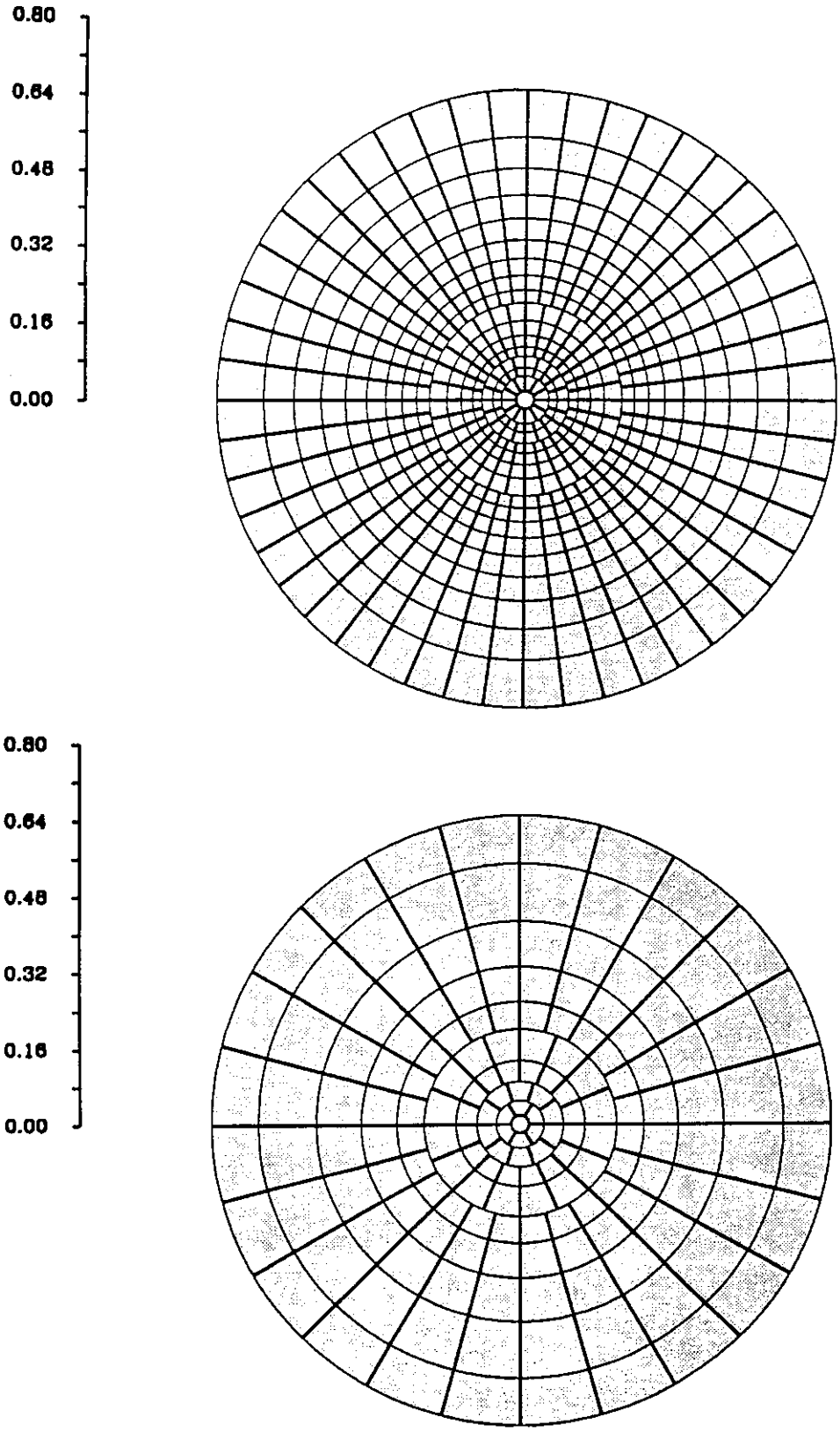

Figure 4

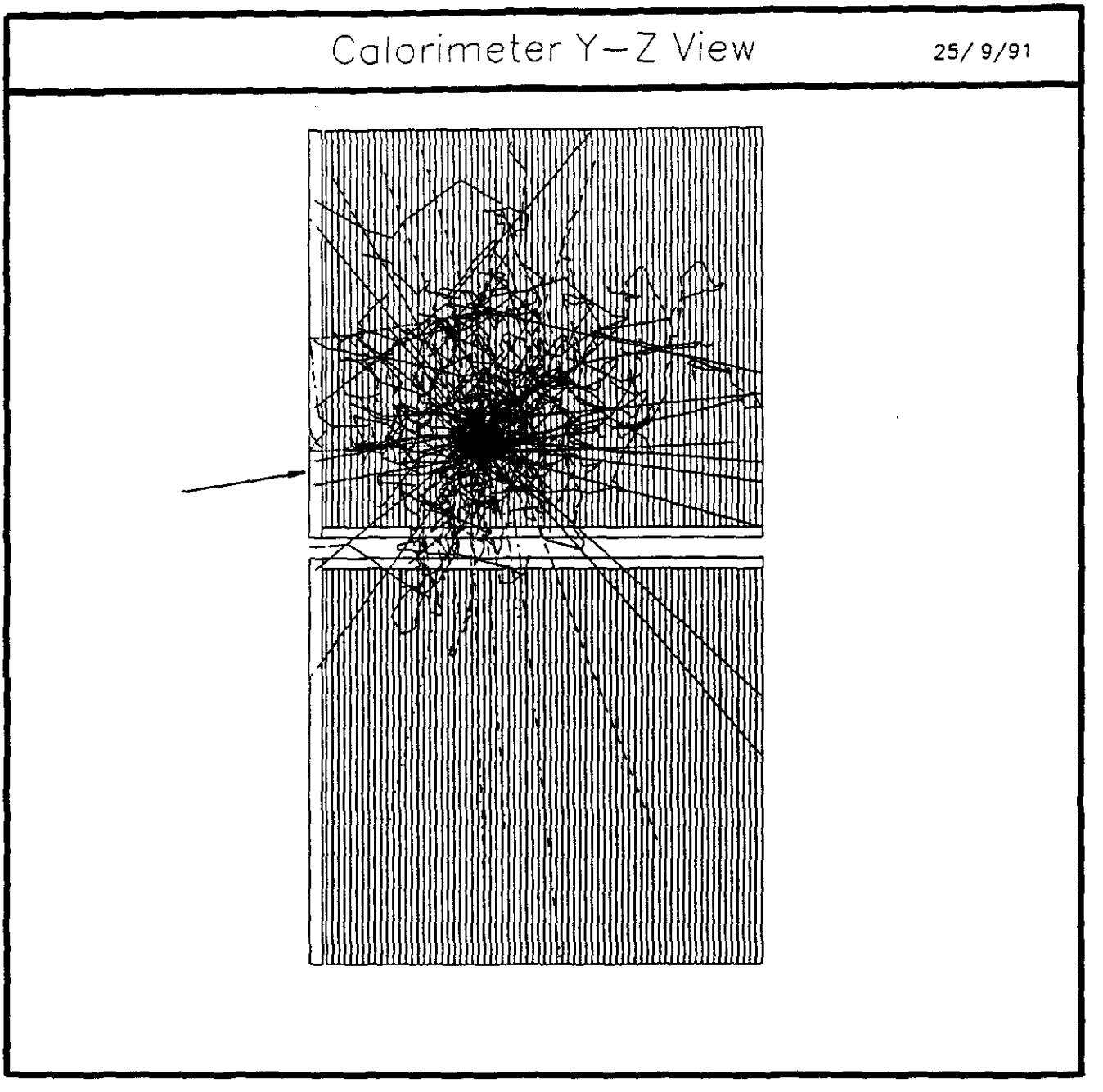

Figure 5

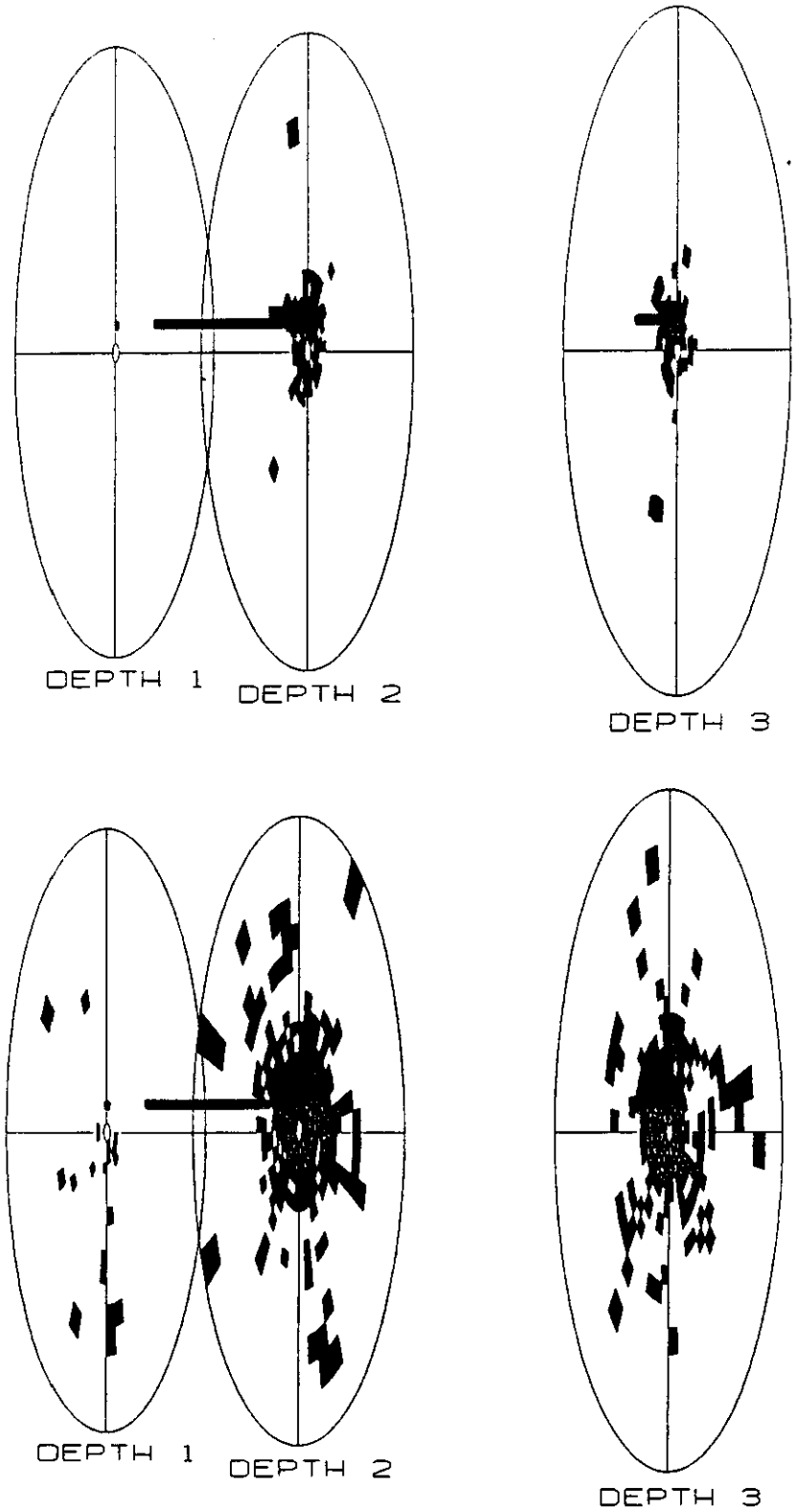

Figure 6

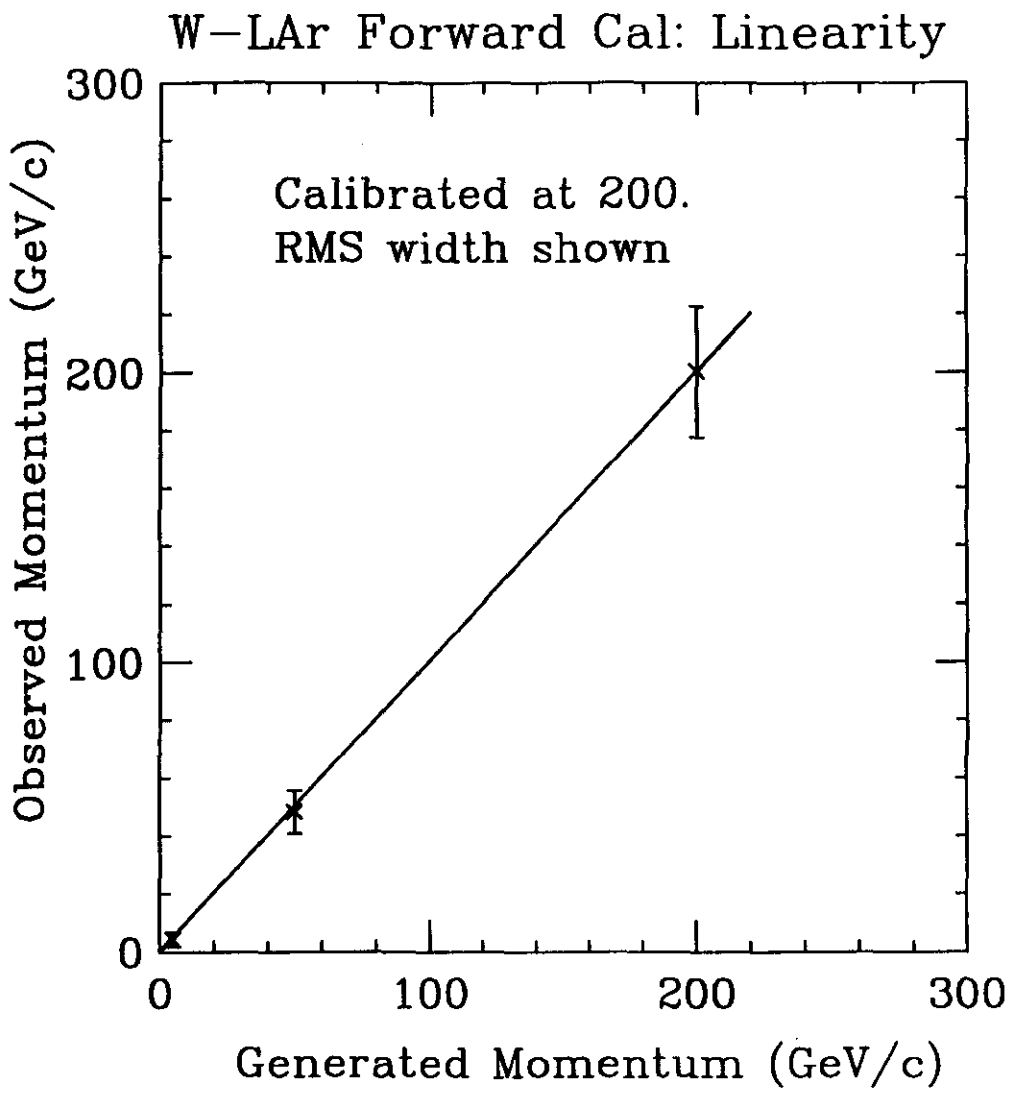
W−LAr Forward Cal: Linearity
Calibrated at 200.
RMS width shown
Observed Momentum (GeV/c)
Generated Momentum (GeV/c)
0
100
200
300
0
100
200
300

Figure 7

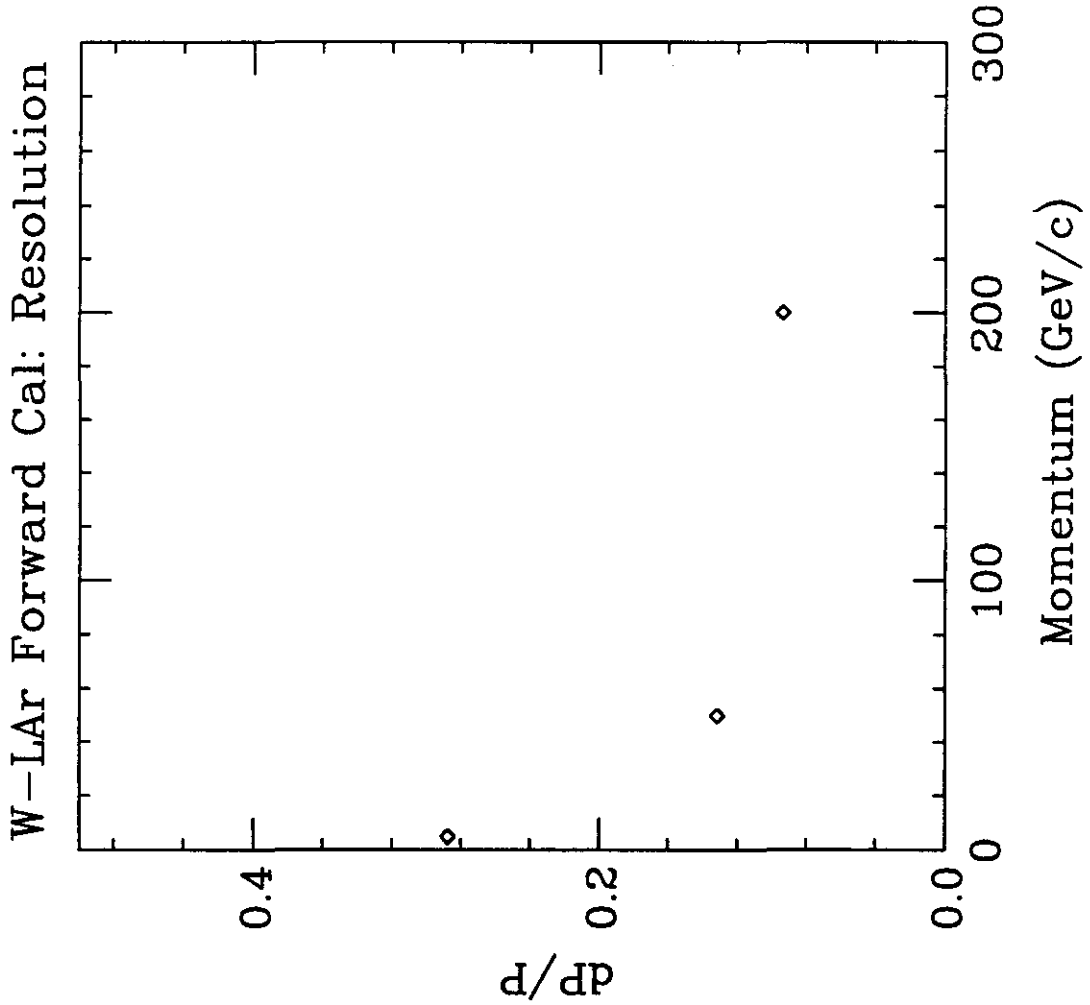
W−LAr Forward Cal: Resolution
dP/P
0.0
0.2
0.4
0
100
200
300
Momentum (GeV/c)

Figure 8

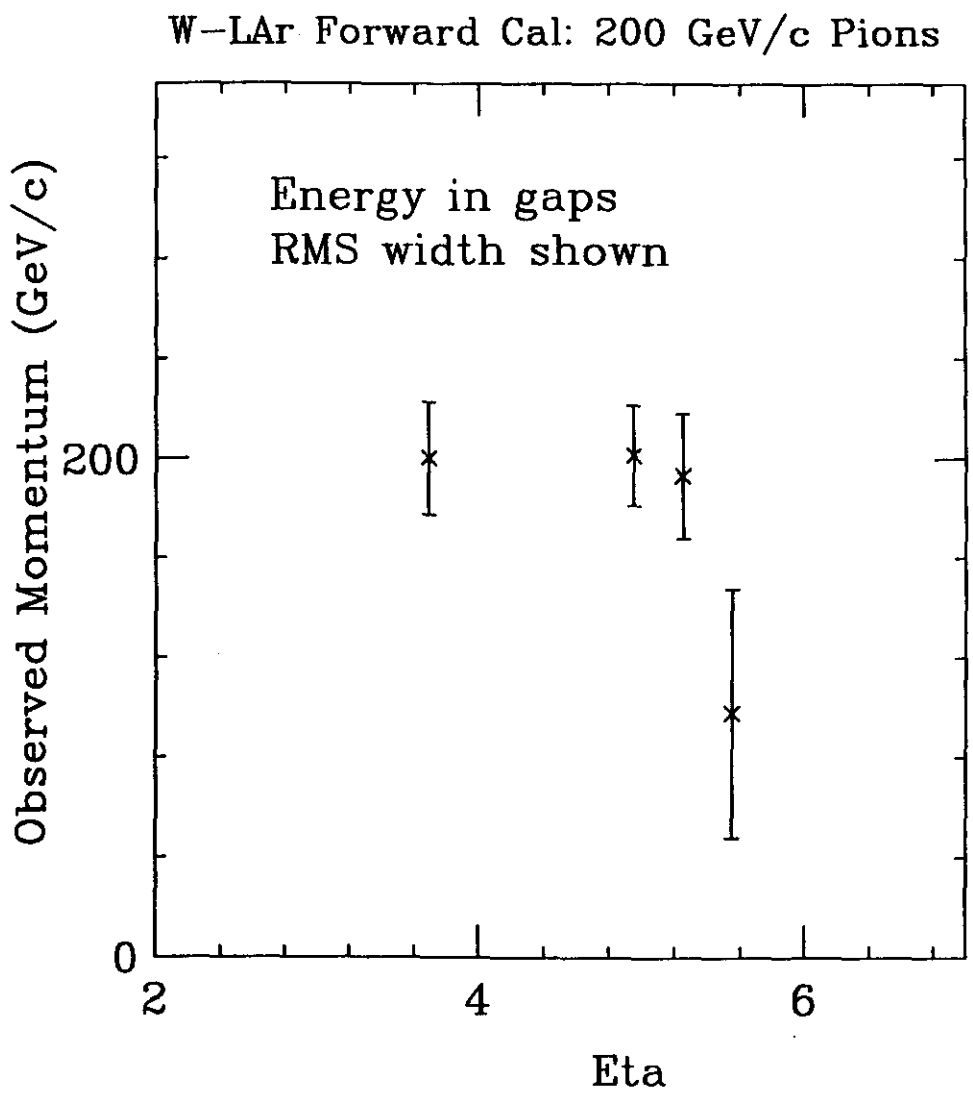
W-LAr Forward Cal: 200 GeV/c Pions
Energy in gaps
RMS width shown
Observed Momentum (GeV/c)
200
0
2
4
6
Eta

Figure 9

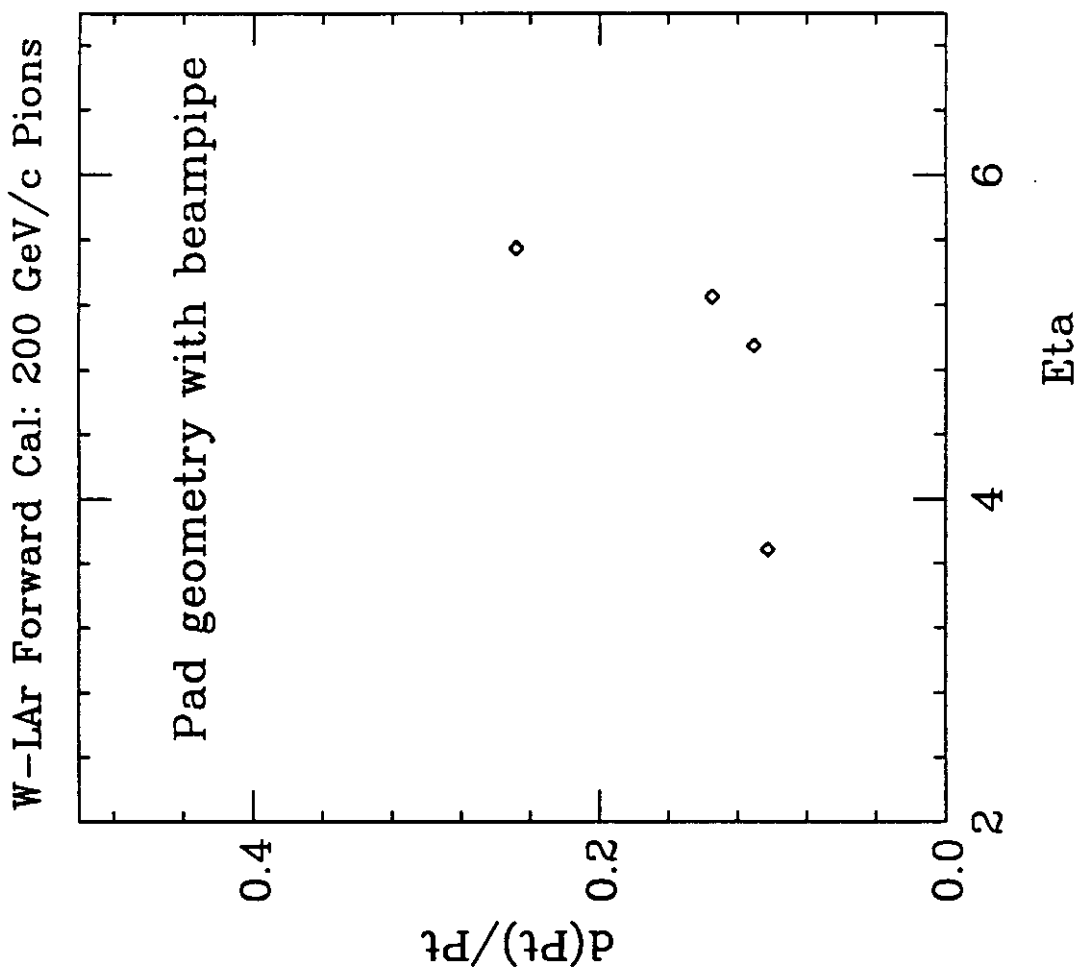
W-LAr Forward Cal: 200 GeV/c Pions
Pad geometry with beampipe
d(Pt)/Pt
0.0
0.2
0.4
2
4
6
Eta

Figure 10